Impact of fluorine on the thermal stability of phlogopite

Jiaqui Sun, Yan Yang, Jannick Ingrin, Zhongping Wang, Qunke Xia

This is the peer-reviewed, final accepted version for American Mineralogist, published by the Mineralogical Society of America.
The published version is subject to change. Cite as Authors (Year) Title. American Mineralogist, in press.
DOI: https://doi.org/10.2138/am-2022-8051. http://www.minsocam.org/

Revision 2

Impact of fluorine on the thermal stability of phlogopite

JIAQI SUN[1], YAN YANG[1]*, JANNICK INGRIN[2], ZHONGPING WANG[3], and QUNKE XIA[1]

[1]Key Laboratory of Geoscience Big Data and Deep Resource of Zhejiang Province, School of Earth Sciences, Zhejiang University, Hangzhou, China

[2]Univ.Lille, CNRS, INRA, ENSCL, UMR 8207, UMET, Unité Matériaux et Transformations, F 59000 Lille, France

[3]Department of Physics, University of Science and Technology of China, Hefei, China

*Corresponding author: Yan Yang (yanyang2005@zju.edu.cn)

ABSTRACT

Knowledge of volatile cycling is vital to understand evolution of the planet and the life it supports. Although it is gradually accepted that the mantle is a vast store house of H_2O and other volatiles, the impact of co-existing volatiles on the thermal stabilities of OH and the lattice of the host mineral is still poorly understood. Phlogopite is one of the few hydrous minerals capable of carrying both water and halogens into the mantle. Previous observations from both experiments and textural relationships in natural samples have indicated that F-rich phlogopite can be stable under ultra-high-temperature conditions. Here, the impact of F on the thermal stability of phlogopite was investigated via XRD, Raman, and IR spectroscopy from room temperature to 1000 to 1200 °C. Based on the experimental results from a F-poor and a F-rich natural phlogopites, we show that about 4 wt% F can increase the breakdown temperature of phlogopite by 100 °C under ambient pressure. The impact mechanism mainly involves preventing OH and lattice softening at high temperatures. This study reveals the links between F and the behavior of OH and phlogopite lattice, which is important for constraining volatile cycling as well as F's role in the physical and chemical properties of the upper mantle.

Keywords: Fluorine, water, thermal stability, phlogopite, mantle

INTRODUCTION

Volatiles (e.g., hydrogen, nitrogen, carbon, and halogens) are not only present on the surface of the Earth, but also in the deep Earth. Volatile exchange between the surface and mantle plays a critical role in the evolution and habitability of the Earth. Although a large number of studies have investigated volatile cycling in the deep Earth, it is still unclear how these volatiles are transported. Volatile transport in the deep Earth mainly depends on the thermal stabilities of the host minerals (van Keken et al. 2011). Most hydrous minerals are not only important water carriers, but carry also other volatiles such as nitrogen and the halogens (Williams et al. 1992; Bebout 1997; Hall 1999; Sadofsky and Bebout 2000; Yokochi et al. 2009; John et al. 2011; Palya 2011; Kendrick et al. 2013; Halama et al. 2014; Pagé et al. 2016; Grützner et al. 2017a). Few studies have paid attention to the possible links between the volatiles when evaluating volatile transport by the host minerals. It has been noticed that fluorine (F) substituting for hydroxyl (OH) can extend the pressure-temperature stability field of the hydrous minerals such as amphibole, talc, and clinohumite (Foley 1991; Chibisov 2011; Grützner et al. 2017a). Recent studies have also pointed out the intimate links between nitrogen and hydrogen diffusion in phengite (Yang et al. 2017; Liu et al. 2019), providing new insights into water release in the Earth's interior. Therefore, exploring the effects of specific volatiles on water release from the host hydrous minerals is greatly needed in order to understand the associated cycling of volatiles and H_2O.

Phlogopite is a sheet silicate frequently found in mantle nodules brought to the Earth's surface mainly by alkaline basalt and kimberlite lavas (Frey and Prinz 1978; Erlank et al. 1987; Fritschle et al. 2013). Fluorine has been experimentally proven to be compatible in phlogopite, with a F partition coefficient between phlogopite and melt larger than 1 (Flemetakis et al. 2021). Thus, phlogopite acts as an important reservoir and carrier of water and F in the upper mantle despite the fact that it is volumetrically insignificant when compared to olivine and pyroxenes (Frost 2006). Many studies have

57 focused on the *P-T* stability field of phlogopite in different systems. Most importantly,
58 observations from both experiments and textural relationships in natural samples have
59 shown that F-rich phlogopite can be stable up to ultra-high-temperature conditions
60 (Peterson et al. 1991; Dooley and Patño Douce 1996; Motoyoshi and Hensen 2001).
61 However, the impact of F on the stability of phlogopite has never been explored further
62 and many unknowns still exist. For instance, what is the relationship between the
63 proportion of F (F/(F+OH) ratio) in phlogopite and the breakdown temperature down to
64 the atomic level? In addition, it has been reported that dehydrogenation could happen at
65 low temperatures, such as 500 °C, before the breakdown of phlogopite (Chon et al.
66 2006; Ventruti et al. 2009; Zema et al. 2010). But it remains unclear whether F has an
67 impact on the dehydrogenation of phlogopite. These unknowns limit a full
68 understanding of volatile release from phlogopite.

69 In this study, we systematically investigate the effect of F on the thermal stability
70 and dehydrogenation of phlogopite, using high temperature Raman spectroscopy and
71 X-ray diffraction (XRD) to monitor the breakdown processes of the lattice, and high
72 temperature Fourier transform infrared (FTIR) spectroscopy to reveal the behavior of
73 OH with increasing temperature.

74 ## MATERIALS AND METHODS

75 ### Samples

76 The two starting samples are phlogopite crystals from two different localities
77 described in Li et al. (2017). The F-rich phlogopite is a 10 × 5 mm, golden-brown
78 crystal from Franklin, New Jersey, United States. The F-poor phlogopite is a 70 × 50
79 mm, reddish-brown crystal from Badakhshan, Afghanistan. The chemical
80 compositions were obtained using a shimadzu electron probe microanalyzer (EPMA
81 1720) at 15 kV and 10 nA beam with a 5 μm beam diameter. Counting time was 10 s on
82 the peak and 10 s on the background for all elements except F, which was 60 s on peak
83 and 30 s on background. Four to seven points were measured on each phlogopite grain.

The average chemical compositions of the two samples are listed in Table 1. Structure formula was calculated on the basis of 22 cation charges, assuming an anion framework of 10 oxygens and 2(OH+F+Cl), and all Fe as Fe^{2+} (Dymek 1983; Rieder et al. 1998). This results in the following formula $(K_{0.963}Na_{0.015})(Mg_{2.677}Fe_{0.166}Al_{0.059}Mn_{0.002}Ti_{0.015}Cr_{0.009}Ni_{0.003})(Si_{3.067}Al_{0.933})O_{10}[F_{0.905}Cl_{0.016}OH_{1.079}]$ for the F-rich phlogopite (X_F = 0.45), and $(K_{0.911}Na_{0.047})(Mg_{2.723}Fe_{0.026}Al_{0.111}Mn_{0.001}Ti_{0.062}Cr_{0.002}Ni_{0.001})(Si_{2.955}Al_{1.045})O_{10}[F_{0.053}Cl_{0.002}OH_{1.945}]$ for the F-poor phlogopite (X_F = 0.026).

X-ray diffraction spectroscopy (XRD)

To monitor the breakdown processes of the two samples, high temperature X-ray diffraction measurements were carried out on a PANalytical X'Pert PRO Multipurpose Diffractometer (MPD), powered by a Philips PW3040 generator and equipped with an X'Celerator detector using CuKα radiation (λ=1.5406 Å). The measurements were operated at 40 kV and 40 mA with 2θ ranging from 7 to 70°. Both samples were finely pulverized in an agate mortar for over 3 h and then passed through a 74 μm sieve. Powders were mounted on a platinum resistive heating stage and placed in an evacuated chamber. For each run, the temperature was increased from room temperature to 1100 °C at 100 °C intervals and with a heating rate of 10 °C/min. The temperature was monitored by a TCU1000N (2604 unit) controller with a temperature error of less than 1 °C. The XRD spectra were collected at each temperature. Each 100 °C temperature step consisted of a 15 min dwell time and a 30 min detection time. All data were analyzed using the Jade 6 software.

Raman spectroscopy

To further characterize phlogopite breakdown processes, high temperature Raman spectra of the phlogopites in the frequency range 50 to 1200 cm^{-1} were collected using a LABRAM-HR spectrometer with an 1800 grooves/mm grating. The sample was excited by a 532 nm green light from a Spectra Physics Ar ion laser for a total time of

100 s for each data point. Single-crystal silicon was used as the reference spectrum. High temperatures were produced by a Linkam TS1500 heating stage, equipped with a resistance heater and a S type thermocouple. Temperatures were determined with an uncertainty of less than 1 °C. The powder samples (grain size < 74 μm) were heated while continuously purged by Ar and held for 30 min at the desired temperatures of 900, 1000, 1100, and 1200 °C. Raman spectra were measured on the samples after they have been quenched to room temperature. In order to investigate the evolution of lattice vibrations as a function of increasing temperature, temperature-dependent Raman spectra, from room temperature to 1000 °C, were measured on crystal samples in the heating stage. The heating rate was set to be 10 °C/min, and an idle time of 5 min was applied to each experimental temperature.

Fourier transform infrared (FTIR) spectroscopy

To reveal the behavior of OH and dehydrogenation in the two samples at high temperatures, thin cleavage flakes perpendicular to the (001) plane with a thickness of 50 to 130 μm were used for the temperature-dependent FTIR measurements. Polarized and unpolarized FTIR spectra in the frequency range 1000-4000 cm^{-1} were collected with an IR beam direction perpendicular to the (001) plane (i.e., to the layers) using a Nicolet iS50 FTIR spectrometer coupled with a Continuμm microscope. A KBr beam-splitter and a liquid-nitrogen cooled MCT-A detector were applied. A total of 128 scans were accumulated for each spectrum at a 4 cm^{-1} resolution. The aperture size was set to 50 × 50 μm.

High temperatures were produced using an Instec HS1300 heating stage with CaF_2 windows, equipped with a resistance heater and a S type thermocouple. The phlogopite grains were placed on a sapphire plate in the heating stage continuously purged with N_2 gas. The sample temperature was determined with an uncertainty of less than ±1 °C. The FTIR measurements were performed from room temperature to 100 °C and then 1000 °C using an interval of 100 °C. Samples were heated at a rate of 10 °C/min and

held at the desired temperature for 5 min. Background spectra and sample spectra were collected on the same selected area, respectively, for each grain and each temperature.

RESULTS

Stability of F-rich and F-poor phlogopites at high temperatures

Studies on the stabilities of phlogopite in complex systems have long been carried out (Frost 2006 and references therein). They proposed that the stability field and decomposition products depend on the initial chemical compositions of the systems. In this study, the focus is on the role of F during the breakdown of individual phlogopite crystals.

X-ray diffraction patterns at elevated temperatures are shown in Figure 1. With increasing temperature, the intensities of the original diffraction peaks (005) and (003) of the phlogopite decrease, whereas the intensities of the diffraction peaks for forsterite, such as (222), (031) and (120), grow concomitantly (Figs. 1c-d). Both phlogopite samples began to decompose at 1000°C, as indicated by the appearance of the forsterite diffraction peaks. Moreover, most of the phlogopite diffraction peaks disappear at 1100 °C for the F-poor phlogopite, whereas the sharp diffraction peaks (005) and (003) persist for the F-rich phlogopite, indicating the different degrees of breakdown for the two samples. Comparison of the XRD patterns from the two samples before and after the run shows more clearly the different degrees of breakdown (Fig. 1e). These X-ray diffraction results demonstrate that breakdown starts at 1000 °C for both samples, but the F-poor phlogopite completely decomposes at 1100°C, whereas the F-rich phlogopite has only partly decomposed at the same temperature. The breakdown process of the two phlogopites was further characterized by Raman spectra from the quenched powder samples after annealing at different temperatures (Fig. 2). In accordance with observations from the XRD results, the Raman spectra show that both phlogopites start to decompose at 1000 °C as illustrated by the appearance of the characteristic peaks of forsterite at 825 and 857 cm^{-1}. But the breakdown degrees were

different between the two samples. After annealing at 1100 °C, the F-poor phlogopite completely decomposed as indicated by the disappearance of the initial characteristic peaks of phlogopite, while there still exist remnants of these peaks for the F-rich phlogopite. By 1200 °C, the F-rich phlogopite had completely decomposed, according to the Raman spectra in Figure 2, indicating that the breakdown process is faster for the F-poor phlogopite than for the F-rich one.

Lattice of the F-rich and F-poor phlogopites at various temperatures

The thermal behavior of the crystal lattice for the two samples were investigated using temperature-dependent Raman spectra in the range of 50-1200 cm^{-1} up to 1000°C (Fig. 3). Raman modes of the two phlogopite samples are similar to those observed in previous studies (Loh 1973; Clemens et al. 1987; Tlili et al. 1989; McKeown et al. 1999; Tutti et al. 2000), but minor differences exist in band positions of some modes (Fig. 3a). The predominant modes are 193, 281, 327, 358, and 682 cm^{-1} for the F-poor phlogopite, and 193, 277, 320, and 682 cm^{-1} for the F-rich phlogopite. Modes at 193, 277 to 281, 320 to 327, and 682 cm^{-1} appear to correspond to the same modes in both phlogopites. The intensity of the 358 cm^{-1} mode is much stronger for the F-poor phlogopite than the F-rich one, which is in agreement with the fact that it has only been reported in the synthetic pure OH phlogopite (Clemens et al. 1987). Modes at frequencies less than 350 cm^{-1} are generally classified as the lattice modes where long-range T_4O_{10} sheet motions can mix with M2 and (F, OH) displacements. Modes between 350 and 850 cm^{-1} have bond stretch and bend motions with the T_4O_{10} sheets and M2 octahedra. The mode at 682 cm^{-1} is assigned to O3-T-O1 band, which reflects motion along the *z(c)* direction in the structure (McKeown et al. 1999).

No new band in the spectra appears nor disappears at elevated temperatures (Figs. 3b-c). Most lattice modes shift continuously toward lower wavenumbers without apparent turning points, except for some small accidents around 400 to 500 °C for the 193 and 682 cm^{-1} modes (Figs. 3d-h). These small breaks do not support any structural

192 phase transitions occurring during the heating process, although phlogopite has been
193 found to undergo a structural phase transition at temperatures of around 400 °C (Tutti
194 and Lazor 2008). Similarly, Zhang et al. (2016) found that the phonon modes of
195 phlogopite all exhibited gradual changes with increasing temperature except for the
196 Al-O and Si-O stretching vibrations, which show a discontinuity near 327 °C. This was
197 suggested by the authors to be related to the alteration of the OH environment. The
198 small accidents around 400 to 500 °C for the 193 and 682 cm^{-1} modes observed in this
199 study could be related to dehydrogenation processes, which is evidenced by the
200 behavior of OH at elevated temperatures (Fig. 4).

201 **Behavior of OH in F-rich and F-poor phlogopites as a function of temperature**

202 Figures 4a-b show the temperature-dependent unpolarized IR spectra of OH
203 vibrations in the 3500 to 3750 cm^{-1} range up to 1000 °C for the F-rich and F-poor
204 phlogopites. For both samples, the absorptions of OH stretching bands recorded
205 through IR beam perpendicular to the (001) plane have isotropic properties, thus, the
206 spectra with polarizer rotating to different angles are similar (Fig. 4c). Some
207 differences in OH wavenumbers between the two samples can nevertheless be observed.
208 For the F-poor phlogopite, there are mainly three OH bands at 3714, 3671, and 3621
209 cm^{-1}. In contrast, three OH bands at 3707, 3665 and 3599 cm^{-1} are shown in the IR
210 spectra of the F-rich phlogopite. Vedder (1964) divided the OH bands in phlogopite
211 into three groups: type N band (normal) corresponding to OH bonding to three
212 octahedrally coordinated divalent cations, type I band (impurity) related to OH bonding
213 to two divalent and one trivalent cations, and type V band (vacancy) due to an OH
214 adjacent to an octahedral vacancy. All previous studies assign the bands at 3714 and
215 3707 cm^{-1} to the type N OH (Vedder and Wilkins 1969; Zhang et al. 2016). Bands at
216 3671 and 3665 cm^{-1} were assigned to the type I OH, relating to $Mg_2(Al, Fe^{3+})$-OH
217 species (Robert and Kodama 1988; Ventruti et al. 2009; Zhang et al. 2016). The bands
218 at 3621 and 3599 cm^{-1} are generally associated with the type V OH, corresponding to a

vacancy with two divalent ions in the octahedral sheet and a vacancy with one divalent ion and one trivalent ion, respectively (Vedder 1964). The relative intensity of the type N OH to the other two groups is larger for the F-poor phlogopite than the F-rich phlogopite, which is consistent with the conclusion that F prefers to substitute for the type N OH based on analyses of synthetic F-rich phlogopites (Papin et al. 1997).

Since the IR spectra exhibit isotropic features independent of the polarizer orientation in (001) plane, we used only unpolarized IR spectroscopy to study the OH in phlogopite at elevated temperatures. Comparison between the IR spectra of the F-poor phlogopite before heating and after quenching shows no evident decrease of the absorbance for the type N OH (3714 and 3707 cm^{-1}), and a small decrease for the type I OH (3671 and 3665 cm^{-1}), while the type V OH (3621 and 3599 cm^{-1}) almost disappears. These variations in the absorbances suggest dehydrogenation, especially for the type V OH (Figs. 4a-b). We could not tell from the spectra whether dehydrogenation happened at elevated temperatures for the F-rich phlogopite, because the spectrum of the quenched sample from 1000 °C is seriously distorted. But dehydrogenation could be inferred from the evolution of the OH band wavenumbers with temperature. The three OH band groups shift to lower wavenumbers with increasing temperature, but with discontinuities at 400 to 500 °C for the type I OH and the type V OH bands (Fig. 4d). The abrupt shift in the temperature-induced OH wavenumber for type I OH and type V OH, observed around 400 to 500 °C, occurs in the temperature range where dehydrogenation is generally observed in phlogopite (e.g., Vedder and Wilkins 1969; Tutti et al. 2000; Zhang et al. 2016). Thus, both phlogopites experienced dehydrogenation of type I OH and type V OH at around 400 to 500 °C during heating, further confirming the IR spectra before heating and after quenching, although we cannot confirm it with the spectrum from the quenched F-rich phlogopite.

DISCUSSION

The effects of F on the thermal stability of phlogopite

It has already been documented that F may markedly extend the thermal stability of phlogopite. For example, the experimental study by Hensen and Osanai (1994) demonstrated that synthetic phlogopite with about 6 wt% F decomposed at 1045 °C and 9 kbar. Moreover, Dooley and Patiño Douce (1996) found that the synthetic phlogopite with 8.7 wt% F can be stable at 1263 °C at 10 kbar. Accordingly, F-rich phlogopite was reported as a stable constituent in ultra-high-temperature rocks (Motoyoshi and Hensen 2001). To reveal the relationship between F and the breakdown temperature of phlogopite, we plotted the breakdown temperature to proportion of F (F/(F+OH) ratio) in Figure 5 based on the data from this study and previous studies. It shows that addition of F can increase the breakdown temperature, confirming the higher stabilities of F-rich phlogopites previously observed. The F-poor and F-rich phlogopite samples start to decompose at 1000 °C under ambient pressure. But the breakdown process is faster for the F-poor phlogopite compared to the F-rich phlogopite, since the complete breakdown temperature is at least 100 °C lower for the F-poor phlogopite compared with the F-rich phlogopite.

It should be noted that in addition to F, the chemical compositions of these two phlogopites differ. Previous studies have suggested that Ti can stabilize biotite both at high *P-T* and at low H_2O activity (Henry et al. 2005; Harlov et al. 2006; Hansen and Harlov 2007). As basically the Mg endmember of the biotite series, phlogopite should also be stabilized by Ti. To check the effect of Ti on the thermal stability of phlogopite, we plotted the Ti contents vs. the breakdown temperatures of the samples from Figure 5 in the supplementary material (Fig. S1). Indeed, a high Ti content can increase the thermal stability of phlogopite as well. Although the F-poor phlogopite contains more Ti than the F-rich phlogopite, F content still plays an important role in phlogopite stability as shown in Figure 5. Therefore, the actual effect of F on phlogopite could be even stronger if the Ti content was the same in both phlogopite samples. On the other

hand, pressure effect on the mineral stability is also important. To check the effect of F on the breakdown temperature of phlogopite under different pressures, compiled data previously reported for phlogopite and other hydrous minerals at high pressure is plotted in Figure 5. It is shown that F generally plays an important role on the thermal stabilities of the host minerals at the same pressure. For phlogopite, the breakdown temperature increases with the increasing F content no matter whether at ambient pressure or at 7 to 15 kbar. Moreover, the breakdown temperatures of phlogopites with the same amount of F are higher at ambient pressure than at high pressures. Considering the impact of Ti on the phlogopite samples with higher Ti contents used in experiments at 7 to 15 kbar, the breakdown temperatures may be even lower than those shown in Figure 5. Thus, it seems that pressure plays a negative role in the thermal stability of phlogopite, which is the reverse of F effect. However, this pressure effect for phlogopite is not applicable to other minerals. For example, for clinohumite, with a F fraction of 0.5, can be stable up to 1100 °C at 30 kbar (Fig. 5), and up to 1600 °C at 10 GPa as inferred from Grützner et al. (2017).

The effects of F on the breakdown process at high temperatures

With increasing temperature, most Raman modes shift toward lower wavenumbers (Figs. 3d-h), indicating a temperature-induced softening of the phlogopite lattice for the two samples. So far, no one has reported the effect of F on the lattice vibrations of phlogopite at high temperatures. To investigate this, Figure 6a compares the temperature-induced shifts of the main Raman modes of the F-poor phlogopite and the F-rich one. It is seen that F has an impact on the temperature-induced shifts of the modes around 320 and 682 cm^{-1}. The shifted amplitudes of these modes are drastically reduced for the F-rich sample. This suggests that incorporation of F retards the lattice softening at high temperatures.

Fluorine appears to have an impact on the thermal behavior of OH in phlogopite. It can be observed that wavenumbers of the three groups OH bands in the F-rich

phlogopite are generally lower than those in the F-poor phlogopite (Fig. 4d). Relationship between the OH wavenumbers for the three groups of OH bands and Al content has been reported by Robert and Kodama (1988). According to them, micas with higher Al contents show lower OH wavenumbers for the type N and I OH bands, which is in contrast with our study that the F-poor phlogopite with a higher Al content has a higher OH wavenumber for all the types of OH bands. Therefore, the Al content alone cannot explain the differences in OH wavenumbers between the two samples. Another factor may be the higher Fe content in the F-rich phlogopite which will decrease the OH wavenumber (Vedder 1964). In addition, the impact of F on the OH wavenumber has been reported for mica, amphibole, and talc (Robert et al. 1993, 1999; Rywak and Burlitch 1996), which is not difficult to understand considering the stronger electronegativity of F than oxygen (Pauling 1932). Thus, it may be expected that F substitution for OH in phlogopite will strengthen the hydrogen bonding (O-H···F), thereby reducing the OH wavenumber (Libowitzky 1999). This has been seen in the F-induced OH band shift to lower wavenumbers in apatite (e.g., Tacker 2004). To explore the correlation between F incorporation and hydrogen bonding strength, we plot wavenumbers of the type N OH against the F content represented by their X_F values in Figure 6b, based on the data from this study and a compilation of data from literature. Although the data are somewhat scattered, mainly due to different chemical compositions besides F, the negative relationship is obvious. Consequently, with increasing F substitution, the strength of hydrogen bonding in phlogopite will be enhanced. This strengthened hydrogen bonding may influence the thermal stability of OH, which is seen in the different thermal behavior of OH for the F-poor phlogopite vs. F-rich phlogopite. With increasing temperature, the OH bands all become broader, and shift towards lower wavenumbers, suggesting temperature-induced OH softening (Figs. 4a-b). There also exist some differences in the amplitudes of the temperature-induced wavenumber shifts of the OH bands between the two samples. The shift amplitudes are generally larger for the F-poor phlogopite than for the F-rich one (Fig. 6c). In other

328 words, despite the fact that a higher temperature induces OH softening for all the
329 phlogopite samples, phlogopite will experience less softening with addition of F. Thus,
330 dehydrogenation may be more difficult for the F-rich phlogopite, and this needs to be
331 verified by dehydrogenation kinetics studies in future.

332 From the vibrational spectra, the isobaric Grüneisen parameters of the lattice and
333 OH modes in the two samples are calculated via the equation $\gamma_{iP} = -\frac{1}{\alpha \nu_i}(\frac{\partial \nu_i}{\partial T})_P$, where
334 γ_{iP} is isobaric Grüneisen parameter of a mode (ν_i), and α is the thermal expansion
335 coefficient. Since there has been no report of the effects of F on the thermal expansion
336 coefficient of phlogopite, we here refer to the thermal expansion coefficient of $6.26 \times$
337 10^{-5} K^{-1} from Tutti et al. (2000). The calculated isobaric Grüneisen parameters of the
338 two samples are listed in Tables 2 and 3. The parameters are generally larger for the
339 F-poor phlogopite than the F-rich phlogopite, indicating that the OH and lattice of the
340 F-poor phlogopite are more sensitive to temperature. Therefore, our study reveals that
341 both OH and the lattice of F-rich phlogopite have a higher thermal stability, compared
342 with those of the F-poor phlogopite. Hydrogen diffusion from the lattice has been
343 suggested to control the stability of muscovite (Gaines and Vedder 1964). The impact
344 of F on the lattice and the OH are thus probably responsible for the different breakdown
345 processes of the F-rich and F-poor phlogopites at high temperatures. To date, one study
346 has reported on the high-pressure Raman spectra of phlogopite (Williams et al. 2012).
347 They reported that both OH and lattice stiffened with increasing pressure, whereas the
348 impact of F is unknown. Considering that pressure is another important parameter,
349 future experimental work should focus on high pressures to explore the effects of F on
350 the behavior of OH and the lattice of the phlogopite.

351 **IMPLICATIONS**

352 Because of the size similarity between F and OH, it is generally supposed that
353 the incorporation of F into both nominally hydrous and anhydrous silicate minerals is
354 mainly through the substitution for OH (e.g., Robert et al. 1999; Crépisson et al. 2014;

355 Roberge et al. 2015; Beyer et al. 2016; Grützner et al. 2017b; Yoshino and Jaseem
356 2018; Hughes and Pawley 2019). This substitution inevitably causes variations in the
357 structure and property of the phlogopite. The data from this study demonstrates that
358 increasing the F substitution in phlogopite can prevent O-H bonding weakening and
359 lattice softening at high temperatures, and consequently stabilize the phlogopite,
360 which has an impact on the stability of phlogopite at high temperatures.

361 It is well known that the mantle is a major water reservoir in the Earth because of
362 the storage of hydrogen defects in nominally anhydrous mantle minerals such as
363 olivine (e.g., Bell and Rossman 1992; Pearson et al. 2014). Recent studies have also
364 indicated that the mantle has acted as a reservoir for F (e.g., Beyer et al. 2016;
365 Grützner et al. 2018; Yoshino and Jaseem 2018). A close association between F and
366 OH has been demonstrated via their coupled incorporation mechanism in olivine
367 (Crépisson et al. 2014). To date, only one study has reported on the impact of F on
368 nominally anhydrous mantle minerals, mainly focusing on F storage and phase
369 stability (Grützner et al. 2018). Phlogopite is a F-rich and hydrous key mineral in the
370 upper mantle. Experimental studies have suggested that F concentrates preferentially
371 in phlogopite compared to other minerals (Edgar and Charbonneau 1991). The F
372 contents in mantle phlogopites are mostly from 0 to ~5 wt% and some are up to
373 ~8-9.5 wt% (Li et al. 2016). Figure 5 indicates that $X_F > 0.5$ can increase the
374 breakdown temperature of phlogopite to over 100 °C under ambient pressure.
375 Considering the high-pressure conditions in the upper mantle and the impact of other
376 elements, such as Ti, the specific breakdown temperature for phlogopite would be
377 affected. For example, a phlogopite with 8 wt% F ($X_F = 0.9$) is expected to be stable
378 up to 1350 °C under ambient pressure, while it is expected to be stable up to a
379 temperature lower than 1300°C at 7-15 kbar (Fig. 5). Indeed, high-Ti phlogopite
380 containing 8 wt% F has been found in an ultra-high-temperature (UHT) metamorphic
381 terrane (980-1120 °C, below 9 kbar) (Motoyoshi and Hensen 2001) suggesting that
382 F-rich samples can be stable at higher temperatures at ambient pressure than at a

higher pressure. Consequently, the increased stability and hydrogen bonding of F-bearing phlogopite makes it an excellent candidate for the storage and transport of both H_2O and the halogens in the upper mantle. In the lithospheric mantle, F can be stored both in hydrous minerals and nominally anhydrous minerals. Although amphibole, phlogopite, and apatite are accessory mantle phases, they are dominant F carriers because F is likely a compatible element in these minerals (Klemme and Stalder 2018). Furthermore, the transport of F in the mantle is dependent on the thermal stabilities of F-bearing minerals. Previous studies showed that phlogopite can be stable up to 1100 °C under 6 GPa, amphibole (K-richterite) can be stable up to 1300 °C, and apatite can be stable up up to 1100 °C under 6 to 8 GPa (Konzett and Ulmer 1999; Konzett et al. 2012). Since F plays an important role in stabilizing phlogopite, amphibole, and apatite (e.g., Frost 2006), F-bearing phlogopite, amphibole, and apatite act as important repositories of F in the mantle, dependent on their distributions in some regional zones.

The effect of F on the hydrogen bonding may have some implications on the dehydrogenation and electrical conductivity of phlogopite. Although it has been reported that dehydrogenation will occur before phlogopite breaks down (e.g., Vedder and Wilkins 1969; Tutti et al. 2000; Zhang et al. 2016), our study shows that the addition of F may make dehydrogenation more difficult. Furthermore, Li et al. (2017) has reported that increasing the F content can significantly enhance the electrical conductivity of phlogopite. Our study shows that F incorporation can prevent O-H bonds from weakening at high temperatures, which may impede hydrogen mobility. Therefore, the contribution of hydrogen conductivity should decrease with increasing F content in phlogopite.

ACKNOWLEDGMENTS

This work is supported by the National Natural Science Foundation of China

(41972038), the Zhejiang Province Natural Science Foundation of China (LY18D020001), and the Fundamental Research Funds for the Central Universities (K20210168). Can Rao and Suwen Qiu are thanked for the analysis of F using EPMA.

REFERENCES

Bebout, G.E. (1997) Nitrogen isotope tracers of high-temperature fluid-rock interactions: Case study of the Catalina Schist, California. Earth and Planetary Science Letters, 151(1-2), 77-90.

Bell, D.R., and Rossman, G.R. (1992) Water in Earth's Mantle: The Role of Nominally Anhydrous Minerals. Science, 255, 1391-1397.

Beyer, C., Klemme, S., Grützner, T., Ireland, T.R., Magee, C.W., and Frost, D.J. (2016) Fluorine partitioning between eclogitic garnet, clinopyroxene, and melt at upper mantle conditions. Chemical Geology, 437, 88-97.

Chibisov, A.N. (2011) Effect of Fluorine Additions on the Stability of $Mg_3Si_4O_{10}(OH)_2$: Computer Simulation. Glass Physics and Chemistry, 37(4), 441-444.

Chon, C.M., Lee, C.K., Song, Y., and Kim, S.A. (2006) Structural changes and oxidation of ferroan phlogopite with increasing temperature: in situ neutron powder diffraction and Fourier transform infrared spectroscopy. Physics and Chemistry of Minerals, 33(5), 289-299.

Clemens, J.D., Circone, S., Navrotsky, A., McMillan, P.F., Smith, B.K., and Wall, V.J. (1987) Phlogopite: High temperature solution calorimetry, thermodynamic properties, Al-Si and stacking disorder, and phase equilibria. Geochimica et Cosmochimica Acta, 51(9), 2569-2578.

Crépisson, C., Blanchard, M., Bureau, H., Sanloup, C., Withers, A.C., Khodja, H., Surblé, S., Raepsaet, C., Béneut, K., Leroy, C., Giura, P., and Balan, E. (2014) Clumped fluoride-hydroxyl defects in forsterite: Implications for the upper-mantle. Earth and Planetary Science Letters, 390, 287-295.

Dooley, D.F., and Patño Douce, A.E. (1996) Fluid-absent melting of F-rich phlogopite + rutile + quartz. American Mineralogist, 81(1-2), 202-212.

Dymek, R.F. (1983) Titanium, aluminum and interlayer cation substitutions in biotite from high-grade gneisses, West Greenland. American Mineralogist, 68(9-10), 880-899.

Edgar, A.D., and Charbonneau, H.E. (1991) Fluorine-bearing phases in lamproites. Mineralogy and Petrology, 44(1-2), 125-149.

443 Erlank, A.J., Waters, F.G., Hawkesworth, C.J., Haggerty, S.E., Allsopp, H.L., Rickard,
444 R.S., and Menzies, M.A. (1987) Evidence for mantle metasomatism in peridotite
445 nodules from the Kimberley pipes, South Africa. In Mantle Metasomatism;
446 Menzies, M.A., Hawkesworth, C.J., Eds.; Academic Press: London, UK; pp. 221–
447 311.

448 Flemetakis, S., Klemme, S., Stracke, A., Genske, F., Berndt, J., and Rohrbach, A. (2021)
449 Constraining the presence of amphibole and mica in metasomatized mantle
450 sources through halogen partitioning experiments. Lithos, 380-381, 1-14.

451 Foley, S. (1991) High-pressure stability of the fluor- and hydroxy-endmembers of
452 pargasite and K-richterite. Geochimica et Cosmochimica Acta, 55(9), 2689-2694.

453 Frey, F.A., and Prinz, M. (1978) Ultramafic inclusions from San Carlos, Arizona:
454 Petrologic and geochemical data bearing on their petrogenesis. Earth and
455 Planetary Science Letters, 38(1), 129-176.

456 Fritschle, T., Prelević, D., Foley, S.F., and Jacob, D.E. (2013) Petrological
457 characterization of the mantle source of Mediterranean lamproites: Indications
458 from major and trace elements of phlogopite. Chemical Geology, 353, 267-279.

459 Frost, D.J. (2006) The Stability of Hydrous Mantle Phases. Reviews in Mineralogy and
460 Geochemistry, 62(1), 243-271.

461 Gaines, G.L., and Vedder, W. (1964) Dehydroxylation of muscovite. Nature, 201, 495.

462 Grützner, T., Klemme, S., Rohrbach, A., Gervasoni, F., and Berndt, J. (2017a) The role
463 of F-clinohumite in volatile recycling processes in subduction zones. Geology,
464 45(5), 443-446.

465 Grützner, T., Kohn, S.C., Bromiley, D.W., Rohrbach, A., Berndt, J., and Klemme, S.
466 (2017b) The storage capacity of fluorine in olivine and pyroxene under upper
467 mantle conditions. Geochimica et Cosmochimica Acta, 208, 160-170.

468 Grützner, T., Klemme, S., Rohrbach, A., Gervasoni, F., and Berndt, J. (2018) The effect
469 of fluorine on the stability of wadsleyite: implications for the nature and depths of
470 the transition zone in the Earth's mantle. Earth and Planetary Science Letters, 482,
471 236-244.

472 Halama, R., Bebout, G.E., John, T., and Scambelluri, M. (2014) Nitrogen recycling in
473 subducted mantle rocks and implications for the global nitrogen cycle.
474 International Journal of Earth Sciences, 103(7), 2081-2099.

475 Hall, A. (1999) Ammonium in granites and its petrogenetic significance. Earth-Science
476 Reviews, 45(3), 145-165.

Hammouda, T., Pichavant, M., Barbey, P., and Brearley, A. (1995) Synthesis of fluorphlogopite single crystals. Applications to experimental studies. European Journal of Mineralogy, 7(6), 1381-1387.

Hansen, E.C., and Harlov, D.E. (2007) Whole-rock, phosphate, and silicate compositional trends across an amphibolite- to granulite-facies transition, Tamil Nadu, India. Journal of Petrology, 48(9), 1641-1680.

Harlov, D.E., Johansson, L., Kerkhof, A.V.D., and Förster, H.-J. (2006) The role of advective fluid flow and diffusion during localized, solid-state dehydration: Sörndrum Stenhuggeriet, Halmstad, SW Sweden. Journal of Petrology, 47(1), 3-33.

Henry, D.J., Guidotti, C.V., and Thomson, J.A. (2005) The Ti-saturation surface for low-to-medium pressure metapelitic biotites: implications for geothermometry and Ti-substitution mechanisms. American Mineralogist, 90, 316-328.

Hensen, B.J., and Osanai, Y. (1994) Experimental Study of Dehydration Melting of F-Bearing Biotite in Model Pelitic Compositions. Mineralogical Magazine, 58A(1), 410-411.

Holloway, J.R., and Ford, C.E. (1975) Fluid-absent melting of the fluoro-hydroxy amphibole pargasite to 35 Kbar. Earth and Planetary Science Letters, 25, 44-48.

Hughes, L., and Pawley, A. (2019) Fluorine partitioning between humite-group minerals and aqueous fluids: implications for volatile storage in the upper mantle. Contributions to Mineralogy and Petrology, 174, 78, 1-18.

John, T., Scambelluri, M., Frische, M., Barnes, J.D., and Bach, W. (2011) Dehydration of subducting serpentinite: Implications for halogen mobility in subduction zones and the deep halogen cycle. Earth and Planetary Science Letters, 308(1-2), 65-76.

Kendrick, M.A., Honda, M., Pettke, T., Scambelluri, M., Phillips, D., and Giuliani, A. (2013) Subduction zone fluxes of halogens and noble gases in seafloor and forearc serpentinites. Earth and Planetary Science Letters, 365, 86-96.

Klemme, S., and Stalder, R. (2018) Halogens in the Earth's Mantle: What We Know and What We Don't. In: Harlov D., Aranovich L. (eds) The Role of Halogens in Terrestrial and Extraterrestrial Geochemical Processes. Springer Geochemistry. Springer, Cham.

Konzett, J., and Ulmer, P. (1999) The stability of hydrous potassic phases in lherzolitic mantle-an experimental study to 9.5 GPa in simplified and natural bulk compositions. Journal of Petrology, 40, 629-652.

Konzett, J., Rhede, D., and Frost, D.J. (2012) The high PT stability of apatite and Cl partitioning between apatite and hydrous potassic phases in peridotite: an

experimental study to 19 GPa with implications for the transport of P, Cl and K in the upper mantle. Contributions to Mineralogy and Petrology, 163, 277-296.

Lacalamita, M., Schingaro, E., Scordari, F., Ventruti, G., Fabbrizio, A., and Pedrazzi, G. (2011) Substitution mechanisms and implications for the estimate of water fugacity for Ti-rich phlogopite from Mt. Vulture, Potenza, Italy. American Mineralogist, 96(8-9), 1381-1391.

Li, Y., Jiang, H., and Yang, X. (2017) Fluorine follows water: Effect on electrical conductivity of silicate minerals by experimental constraints from phlogopite. Geochimica et Cosmochimica Acta, 217, 16-27.

Li, Y., Yang, X., Yu, J.-H., and Cai, Y.-F. (2016) Unusually high electrical conductivity of phlogopite: the possible role of fluorine and geophysical implications. Contributions to Mineralogy and Petrology, 171(4), 37.

Libowitzky, E. (1999) Correlation of O-H stretching frequencies and O-H···O hydrogen bond lengths in minerals. Monatshefte für Chemie, 130, 1047-1059.

Liu, W., Yang, Y., Busigny, V., and Xia, Q.-K. (2019) Intimate link between ammonium loss of phengite and the deep Earth's water cycle. Earth and Planetary Science Letters, 513, 95-102.

Loh, E. (1973) Optical vibrations in sheet silicates. Journal of Physics C: Solid State Physics, 6(6), 1091-1104.

McKeown, D.A., Bell, M.I., and Etz, E.S. (1999) Raman spectra and vibrational analysis of the trioctahedral mica phlogopite. American Mineralogist, 84(5-6), 970-976.

Motoyoshi, Y., and Hensen, B.J. (2001) F-rich phlogopite stability in ultra-high-temperature metapelites from the Napier Complex, East Antarctica. American Mineralogist, 86, 1404-1413.

Oba, T. (1990) Experimental study on the tremohte-pargasite join at variable temperatures under 10 kbar. Journal of Earth System Science, 99(1), 81-90.

Ogorodova, L.P., Kiseleva, I.A., Mel'chakova, L.V., and Vladykin, N.V. (2009) Thermodynamic properties of natural tetraferriphlogopite. Geochemistry International, 47(11), 1137-1140.

Pagé, L., Hattori, K., de Hoog, J.C.M., and Okay, A.I. (2016) Halogen (F, Cl, Br, I) behaviour in subducting slabs: A study of lawsonite blueschists in western Turkey. Earth and Planetary Science Letters, 442, 133-142.

Palya, A.P. (2011) Storage and mobility of organic nitrogen and carbon in the continental crust: Evidence from partially melted metasedimentary rocks, Mt. Stafford, Australia. Chemical Geology, 281(3), 211-226.

549 Papin, A., Sergent, J., and Robert, J.L. (1997) Intersite OH-F distribution in an Al-rich
550 synthetic phlogopite. European Journal of Mineralogy, 9, 501-508.

551 Pauling, L. (1932) The nature of the chemical bond. IV. The energy of single bonds and
552 the relative electronegativity of atoms. Journal of the American Chemical Society,
553 54, 3570-3582.

554 Pearson, D.G., Brenker, F.E., Nestola, F., McNeill, J., Nasdala, L., Hutchison, M.T.,
555 Matveev, S., Mather, K., Silversmit, G., Schmitz, S., Vekemans, B., and Vincze, L.
556 (2014) Hydrous mantle transition zone indicated by ringwoodite included within
557 diamond. Nature, 507, 221-224.

558 Peterson, J.W., Chacko, T., and Kuehner, S.M. (1991) The effects of fluorine on the
559 vapor-absent melting of phlogopite + quartz; implications for deep-crustal
560 processes. American Mineralogist, 76, 470-476.

561 Piccinini, M., Cibin, G., Marcelli, A., Ventura, G.D., Bellatreccia, F., and Mottana, A.
562 (2006) Synchrotron radiation FT-IR micro-spectroscopy of fluorophlogopite in
563 the O-H stretching region. Vibrational Spectroscopy, 42(1), 59-62.

564 Prost, R., and Laperche, V. (1990) Far-infrared study of potassium in micas. Clays and
565 Clay Minerals, 38(4), 351-355.

566 Rieder, M., Cavazzini, G., D'yakonov, Y.S., Frank-Kamenetskii, V.A., Gottardi, G.,
567 Guggenheim, S., Koval', P.W., Moller, G., Neiva, A.M.R., Radoslovich, E.W.,
568 Robert, J.L., Sassi, F.P., Takeda, H., Weiss, Z., and Wones, D.R. (1998)
569 Nomenclature of the micas. Clays and Clay Minerals, 46, 586-595.

570 Rimsaite, J. (1970) Structural formulae of oxidized and hydroxyl-deficient micas and
571 decomposition of the hydroxyl group. Contributions to Mineralogy and Petrology,
572 25(3), 225-240.

573 Rimsaite, J. (1972) DTA, TG, IR and isotopic analyses and properties of phlogopite,
574 biotite muscovite and lepidolite in temperature range of metamorphic reactions. In:
575 H.G. Wiedemann (Eds.), Thermal Analysis (Vol. 3, pp. 683-695). Basel:
576 Birkhäuser.

577 Roberge, M., Bureau, H., Bolfan-Casanova, N., Frost, D.J., Raepsaet, C., Surble, S.,
578 Khodja, H., Auzende, A., and Fiquet, G. (2015) Is the transition zone a deep
579 reservoir for fluorine? Earth and Planetary Science Letters, 429, 25-32.

580 Robert, J.L., Beny, J.M., Ventura, G., and Hardy, M. (1993) Fluorine in micas:
581 crystal-chemical control of the OH-F distribution between trioctahedral and
582 dioctahedral sites. European Journal of Mineralogy, 5, 7-18.

583 Robert, J.L., and Kodama, H. (1988) Generalization of the correlation between
584 hydroxyl-stretching wavenumbers and composition of micas in the system

585 K_2O-MgO-Al_2O_3-SiO_2-H_2O: a single model for trioctahedral and dioctahedral
586 micas. American Journal of Science, 288(A), 196-212.

587 Robert, J.L., Ventura, G.D., and Hawthorne, F.C. (1999) Near-infrared study of
588 short-range disorder of OH and F in monoclinic amphiboles. American
589 Mineralogist, 84, 86-91.

590 Rywak, A., and Burlitch, J. (1996) The crystal chemistry and thermal stability of
591 sol-gel prepared fluoride-substituted talc. Physics and Chemistry of Minerals, 23,
592 418-431.

593 Sadofsky, S.J., and Bebout, G.E. (2000) Ammonium partitioning and nitrogen-isotope
594 fractionation among coexisting micas during high-temperature fluid-rock
595 interactions: examples from the New England Appalachians. Geochimica et
596 Cosmochimica Acta, 64(16), 2835-2849.

597 Scordari, F., Ventruti, G., Sabato, A., Bellatreccia, F., Ventura, G., and Pedrazzi, G.
598 (2006) Ti-rich phlogopite from Mt. Vulture (Potenza, Italy) investigated by a
599 multianalytical approach: substitutional mechanisms and orientation of the OH
600 dipoles. European Journal of Mineralogy, 18(3), 379-391.

601 Tacker, R.C. (2004) Hydroxyl ordering in igneous apatite. American Mineralogist, 89,
602 1411-1421.

603 Tlili, A., Smith, D.C., Beny, J.-M., and Boyer, H. (1989) A Raman Microprobe Study
604 of Natural Micas. Mineralogical Magazine, 53, 165-179.

605 Tutti, F., Dubrovinsky, L.S., and Nygren, M. (2000) High-temperature study and
606 thermal expansion of phlogopite. Physics and Chemistry of Minerals, 27,
607 599-603.

608 Tutti, F., and Lazor, P. (2008) Temperature-induced phase transition in phlogopite
609 revealed by Raman spectroscopy. Journal of Physics and Chemistry of Solids,
610 69(10), 2535-2539.

611 van Keken, P.E., Hacker, B.R., Syracuse, E.M., and Abers, G.A. (2011) Subduction
612 factory: 4. Depth-dependent flux of H_2O from subducting slabs worldwide.
613 Journal of Geophysical Research, 116(B1).

614 Vedder, W. (1964) Correlations between infrared spectrum and chemical composition
615 of mica. American Mineralogist, 49, 736–768.

616 Vedder, W., and Wilkins, R.W.T. (1969) Dehydroxylation and rehydroxylation,
617 oxidation and reduction of micas. American Mineralogist, 54, 482-509.

618 Ventruti, G., Levy, D., Pavese, A., Scordari, F., and Suard, E. (2009) High-temperature
619 treatment, hydrogen behaviour and cation partitioning of a Fe-Ti bearing volcanic

620 phlogopite by in situ neutron powder diffraction and FTIR spectroscopy.
621 European Journal of Mineralogy, 21(2), 385-396.

622 Weiss, M. (1997) Clinohumites, a field and experimental study. Ph.D. thesis. Zürich,
623 ETH Zür ch, 1-168.

624 Williams, L., Wilcoxon, B.R., Ferrell, R., and Sassen, R. (1992) Diagenesis of
625 ammonium during hydrocarbon maturation and migration, Wilcox Group,
626 Louisiana, U.S.A. Applied Geochemistry, 7, 123-134.

627 Williams, Q., Knittle, E., Scott, H. P., and Liu, Z. (2012) The high-pressure behavior of
628 micas: vibrational spectra of muscovite, biotite, and phlogopite to 30 GPa.
629 American Mineralogist, 97(1), 241-252.

630 Xu, J.S., and Shen, G.F. (2005) Mineralogical study on fluorphlogopite from the Bayan
631 Obo ore deposit. Acta Mineralogica Sinica, 25(3), 213-216 (in Chinese).

632 Yang, Y., Busigny, V., Wang, Z.P., and Xia, Q.K. (2017) The fate of ammonium in
633 phengite at high temperature. American Mineralogist, 102(11), 2244-2253.

634 Yoshino, T., and Jaseem, V. (2018) Fluorine solubility in bridgmanite: A potential
635 fluorine reservoir in the Earth's mantle. Earth and Planetary Science Letters, 504,
636 106-114.

637 Yokochi, R., Marty, B., Chazot, G., and Burnard, P. (2009) Nitrogen in peridotite
638 xenoliths: Lithophile behavior and magmatic isotope fractionation. Geochimica et
639 Cosmochimica Acta, 73(16), 4843-4861.

640 Zema, M., Ventruti, G., Lacalamita, M., and Scordari, F. (2010) Kinetics of
641 Fe-oxidation/deprotonation process in Fe-rich phlogopite under isothermal
642 conditions. American Mineralogist, 95(10), 1458-1466.

643 Zhang, M., Tarantino, S.C., Su, W., Lou, X., Ren, X., Salje, E.K.H., Carpenter, M.A.,
644 and Redfern, S.A.T. (2016) Optical phonons, OH vibrations, and structural
645 modifications of phlogopite at high temperatures: An in-situ infrared
646 spectroscopic study. American Mineralogist, 101(8), 1873-1883.

647

This is the peer-reviewed, final accepted version for American Mineralogist, published by the Mineralogical Society of America.
The published version is subject to change. Cite as Authors (Year) Title. American Mineralogist, in press.
DOI: https://doi.org/10.2138/am-2022-8051. http://www.minsocam.org/

Table 1. Chemical compositions of the two phlogopite samples (in wt%, dash = below 0.01 wt%).

	F-poor phlogopite (from Badakhshan)						**F-rich phlogopite (from Franklin)**								
	Phl1	Phl2	Phl3	Phl4	Average	SD	Phl5	Phl6	Phl7	Phl8	Phl9	phl10	phl11	Average	SD
SiO_2	42.39	43.23	42.67	42.31	42.65	*0.42*	43.16	43.68	43.51	43.69	43.87	43.41	43.52	43.55	*0.23*
TiO_2	1.15	1.13	1.24	1.20	1.18	*0.05*	0.33	0.42	0.18	0.25	0.24	0.23	0.21	0.27	*0.08*
Al_2O_3	14.31	14.18	14.14	14.03	14.16	*0.11*	12.16	11.84	11.87	12.00	12.13	11.85	11.77	11.95	*0.15*
FeO	0.48	0.47	0.41	0.48	0.46	*0.04*	2.80	2.47	2.70	2.73	2.86	2.98	3.17	2.82	*0.22*
MnO	-	0.04	-	0.06	0.02	*0.03*	0.01	0.04	0.01	0.09	0.03	-	0.05	0.03	*0.03*
MgO	26.62	26.34	26.02	26.48	26.37	*0.26*	25.77	25.58	25.88	25.59	25.06	25.36	25.29	25.50	*0.29*
CaO	-	0.01	-	-	-	-	-	-	-	-	-	-	-	-	-
Na_2O	0.30	0.39	0.36	0.35	0.35	*0.03*	0.07	0.09	0.14	0.10	0.12	0.12	0.15	0.11	*0.03*
K_2O	10.36	10.27	10.22	10.41	10.31	*0.09*	10.76	10.77	10.70	10.63	10.71	10.69	10.76	10.72	*0.05*
F	0.23	0.26	0.24	0.24	0.24	*0.01*	3.98	4.10	4.10	4.01	3.97	4.03	4.24	4.06	*0.09*
Cl	-	0.03	0.04	0.02	0.02	*0.02*	0.12	0.12	0.13	0.14	0.16	0.17	0.14	0.14	*0.02*
Cr_2O_3	0.03	-	0.08	0.04	0.04	*0.03*	0.20	0.14	0.13	0.15	0.16	0.14	0.16	0.15	*0.02*
NiO	-	-	-	0.05	0.01	*0.03*	0.07	-	0.05	0.04	0.05	0.08	-	0.04	*0.03*
H_2O*	4.22	4.23	4.19	4.19	4.21		2.34	2.28	2.28	2.33	2.34	2.29	2.20	2.30	
Subtotal	100.08	100.57	99.60	99.85	100.03		101.77	101.52	101.66	101.75	101.70	101.36	101.65	101.63	
O=F,Cl	0.10	0.12	0.11	0.11	0.11		1.70	1.75	1.76	1.72	1.71	1.74	1.81	1.74	
Total	99.99	100.45	99.49	99.74	99.92		100.06	99.77	99.90	100.03	99.99	99.62	99.84	99.89	

Note: *H_2O and OH estimated on the basis of 22 cation charges, assuming 10 oxygen and 2(OH+F+Cl) (Rieder et al. 1998).

This is the peer-reviewed, final accepted version for American Mineralogist, published by the Mineralogical Society of America.
The published version is subject to change. Cite as Authors (Year) Title. American Mineralogist, in press.
DOI: https://doi.org/10.2138/am-2022-8051. http://www.minsocam.org/

652 **Table 2.** Evolutions of wavenumbers of the lattice modes (cm^{-1}) with temperature and the isobaric Grüneisen parameters. The data in italics are the
653 uncertainties.

Temperature (°C)	**F-poor phlogopite Lattice mode (cm^{-1})**					**F-rich phlogopite Lattice mode (cm^{-1})**			
20	192.8	281.3	326.9	357.7	681.6	192.6	276.6	320.4	682.4
	0.29	*0.39*	*0.73*	*0.42*	*0.28*	*0.20*	*0.22*	*0.70*	*0.21*
100	191.7	280.8	325.3	356.4	680.6	191.3	275.2	320.1	681.2
	0.20	*0.29*	*0.26*	*0.08*	*0.27*	*0.12*	*0.33*	*0.35*	*0.31*
200	190.5	279.9	323.3	354.4	679.7	190.0	274.5	319.1	680.3
	0.20	*0.17*	*0.26*	*0.30*	*0.01*	*0.02*	*0.21*	*0.53*	*0.67*
300	189.0	278.5	321.2	352.7	678.2	188.9	273.3	318.3	679.3
	0.06	*0.28*	*0.62*	*0.21*	*0.24*	*0.09*	*0.65*	*0.10*	*0.69*
400	188.2	277.7	319.6	349.9	676.9	187.3	272.0	317.0	678.7
	0.23	*0.44*	*0.21*	*0.13*	*0.36*	*0.35*	*0.52*	*0.73*	*0.23*
500	186.5	276.3	316.8	347.9	674.3	185.5	270.8	315.8	676.9
	0.26	*0.07*	*0.39*	*0.10*	*0.42*	*0.32*	*0.27*	*0.37*	*0.40*
600	185.4	275.5	314.4	346.0	673.3	184.7	270.0	314.9	675.5
	0.21	*0.34*	*0.76*	*0.19*	*0.21*	*0.29*	*0.39*	*0.48*	*0.07*
700	184.5	274.1	311.9	344.0	671.8	183.9	269.0	314.2	674.5
	0.24	*0.20*	*0.23*	*0.05*	*0.21*	*0.20*	*0.66*	*0.37*	*0.04*
800	183.2	273.5	308.6	342.3	670.1	183.1	267.7	312.2	672.8
	0.39	*0.22*	*0.54*	*0.02*	*0.38*	*0.19*	*0.42*	*0.57*	*0.40*
900	181.8	272.4	306.0	340.6	668.6	182.0	266.4	310.8	671.2
	0.19	*0.71*	*0.22*	*0.13*	*0.26*	*0.50*	*0.51*	*1.02*	*0.09*
1000	180.6	271.3	304.0	338.7	667.5	180.7	265.7	309.6	669.2
	0.20	*0.91*	*0.60*	*0.07*	*0.22*	*0.09*	*0.03*	*0.48*	*1.25*
Wavenumber shift with temperature (cm^{-1}/°C)	-0.0128 (20-400°C)	-0.0108 (20-1000°C)	-0.0242 (20-1000°C)	-0.0197 (20-1000°C)	-0.0123 (20-400°C)	-0.0125 (20-400°C)	-0.0109 (20-1000°C)	-0.0114 (20-1000°C)	-0.0097 (20-400°C)
Isobaric Grüneisen parameters	1.061	0.613	1.179	0.880	0.288	1.039	0.630	0.567	0.227

654

This is the peer-reviewed, final accepted version for American Mineralogist, published by the Mineralogical Society of America.
The published version is subject to change. Cite as Authors (Year) Title. American Mineralogist, in press.
DOI: https://doi.org/10.2138/am-2022-8051. http://www.minsocam.org/

655 **Table 3.** Evolutions of wavenumbers of the three groups of OH bands (cm^{-1}) with temperature and the isobaric Grüneisen parameters of the OH modes. The
656 data in italic are the uncertainties.

Temperature (°C)	F-poor phlogopite OH wavenumber (cm^{-1})			F-rich phlogopite OH wavenumber (cm^{-1})		
20	3714.2	3671.3	3621.7	3706.8	3665.5	3599.3
	0.18	*0.25*	*0.20*	*0.22*	*0.51*	*0.61*
100	3711.5	3670.6	3620.8	3704.4	3664.6	3598.0
	0.26	*1.65*	*0.11*	*0.08*	*0.87*	*0.91*
200	3708.7	3670.0	3619.9	3701.7	3664.1	3597.5
	0.14	*0.69*	*0.08*	*0.12*	*0.75*	*0.33*
300	3705.1	3668.0	3618.6	3698.8	3663.0	3596.0
	0.18	*0.31*	*0.16*	*0.14*	*0.46*	*0.88*
400	3701.6	3666.4	3616.6	3695.2	3661.8	3596.0
	0.12	*0.75*	*0.68*	*0.16*	*1.52*	*0.60*
500	3698.5	3662.7	3614.4	3691.6	3659.3	3594.8
	0.04	*1.41*	*1.79*	*0.28*	*1.92*	*0.56*
600	3694.8	3658.9	3607.6	3687.9	3658.1	3583.9
	0.17	*2.25*	*4.06*	*0.33*	*1.64*	*0.55*
700	3691.6	3653.2	3594.4	3685.6	3655.2	3580.4
	0.23	*1.74*	*2.91*	*0.16*	*2.37*	*1.42*
800	3688.2	3650.7	3586.5	3682.8		3581.4
	0.34	*0.35*	*1.53*	*0.27*		*2.19*
900	3684.6			3680.9		
	0.48			*0.16*		
1000	3681.0					
	0.49					
Wavenumber shift with temperature (cm^{-1}/°C)	-0.0336 (20-1000°C)	-0.0119 (20-400°C)	-0.0111 (20-500°C)	-0.0304 (20-900°C)	-0.0089 (20-400°C)	-0.0089 (20-500°C)
Isobaric Grüneisen parameters	0.145	0.052	0.049	0.131	0.039	0.040

657

Figure captions:

Figure 1. (a-b) X-ray diffraction patterns of phlogopite powders at elevated temperatures ("RT" represents room temperature). (c-d) Enlarged regions showing the breakdown processes. (e) Comparison of phlogopite samples before and after the heating and cooling runs.

Figure 2. Comparisons of Raman spectra of lattice vibrations between the initial and quenched powder samples from 900, 1000, 1100, and 1200 °C, respectively. (a-d) F-poor phlogopite; (e-h) F-rich phlogopite. The red arrows indicate the appearance of the characteristic modes of forsterite at 825 and 857 cm^{-1}.

Figure 3. (a) Raman spectra of phlogopites at ambient conditions. (b) Raman spectra at various temperatures from 20 to 1000 °C of the F-poor phlogopite. (c) Raman spectra at various temperatures from 20 to 1000 °C of the F-rich phlogopite. (d-h) Evolution of Raman shifts of lattice modes of the phlogopites (data are in Table 2).

Figure 4. (a) Unpolarized IR spectra of OH stretching vibrations from the F-poor phlogopite at elevated temperatures and quenched from 1000 °C. (b) Unpolarized IR spectra of OH stretching vibrations of F-rich phlogopite at various temperatures and quenched from 1000 °C. The spectrum at 1000 °C of the F-rich phlogopite was corrupt due to serious interference, is not presented here. (c) Unpolarized and polarized IR spectra of OH stretching vibrations at ambient conditions, with the

677 polarizer rotated to 0° and 90° in (001) plane. (d) Wavenumbers of the three groups
678 from unpolarized OH bands with temperature (data from Table 3).

679 Figure 5. Breakdown temperature of phlogopite and other hydrous minerals (pargasite,
680 K-richterite, and clinohumite) as function of F content at different pressures. The blue
681 field represents the phlogopite stability field. Data are from this study and the
682 literature. Phlogopite at ambient pressure: Rimsaite (1970, 1972), Prost and Laperche
683 (1990), Hammouda et al. (1995), Ogorodova et al. (2009). Phlogopite at high
684 pressures: Hensen and Osanai (1994), Dooley and Patiño Douce (1996). Pargasite:
685 Holloway and Ford (1975), Oba (1990). K-richterite: Foley (1991). Clinohumite:
686 Weiss (1997). The open square represents the poorly constrained breakdown
687 temperature of fluorphlogopite in Hammouda et al. (1995). It is probably higher than
688 1403 °C because it completely melts without breakdown at this temperature. The red
689 and blue filled squares represent F-poor and F-rich phlogopites in this study,
690 respectively.

691 Figure 6. (a) Temperature-induced wavenumber shifts of the lattice modes. (b)
692 Wavenumbers of the type N OH at ambient conditions versus X_F. Two data are from
693 this study, and the others are from previous studies (Vedder 1964; Prost and Laperche
694 1990; Xu and Shen 2005; Chon et al. 2006; Piccinini et al. 2006; Scordari et al. 2006;
695 Ventruti et al. 2009; Lacalamita et al. 2011; Zhang et al. 2016). (c)
696 Temperature-induced wavenumber shifts of the OH bands. Since there exist

697 discontinuities in the wavenumber evolutions of some lattice modes and OH bands, the

698 dotted squares indicate the temperature range of the linear fit.

This is the peer-reviewed, final accepted version for American Mineralogist, published by the Mineralogical Society of America.
The published version is subject to change. Cite as Authors (Year) Title. American Mineralogist, in press.
DOI: https://doi.org/10.2138/am-2022-8051. http://www.minsocam.org/

Figure 1

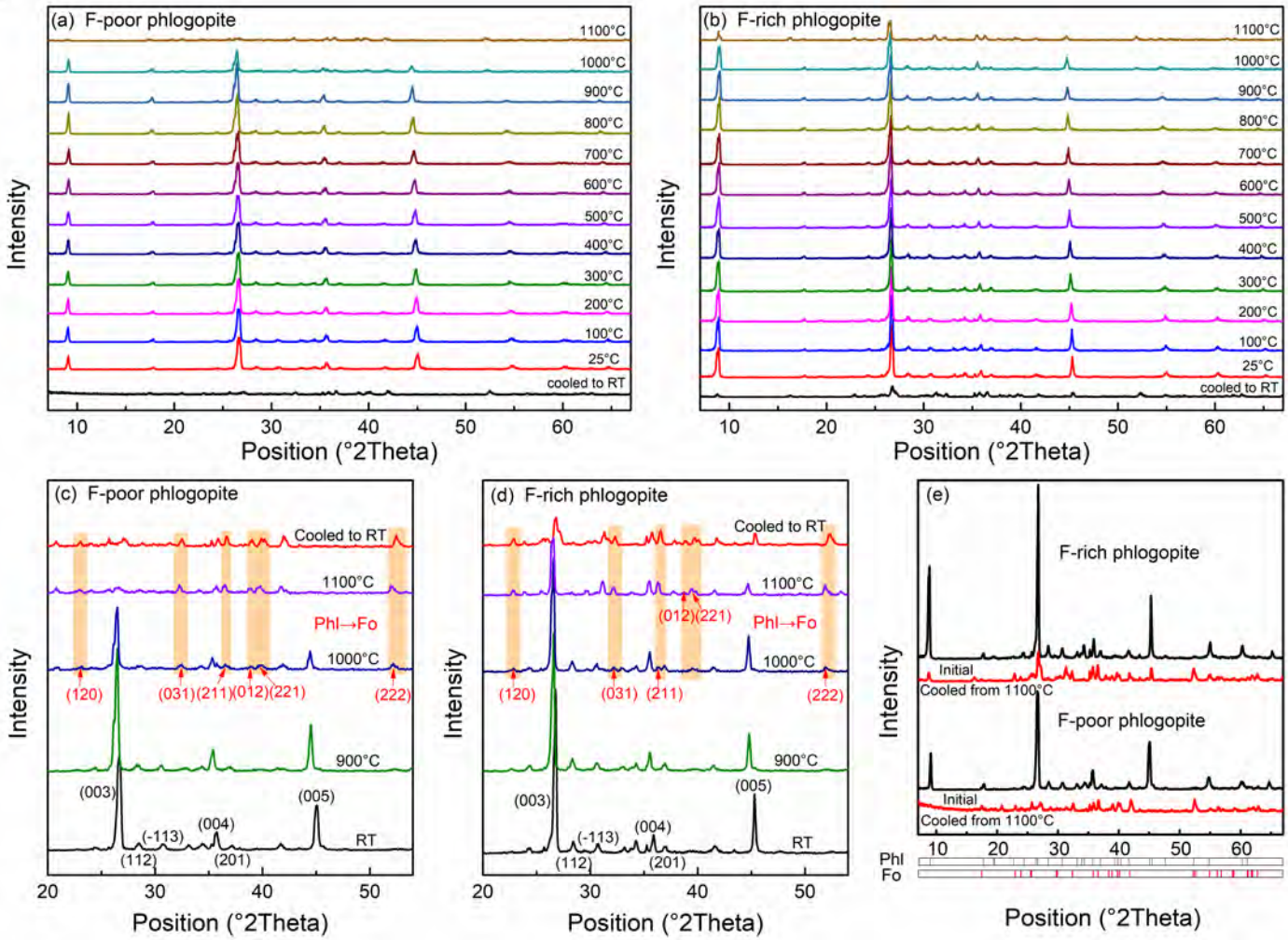

This is the peer-reviewed, final accepted version for American Mineralogist, published by the Mineralogical Society of America.
The published version is subject to change. Cite as Authors (Year) Title. American Mineralogist, in press.
DOI: https://doi.org/10.2138/am-2022-8051. http://www.minsocam.org/

Figure 2

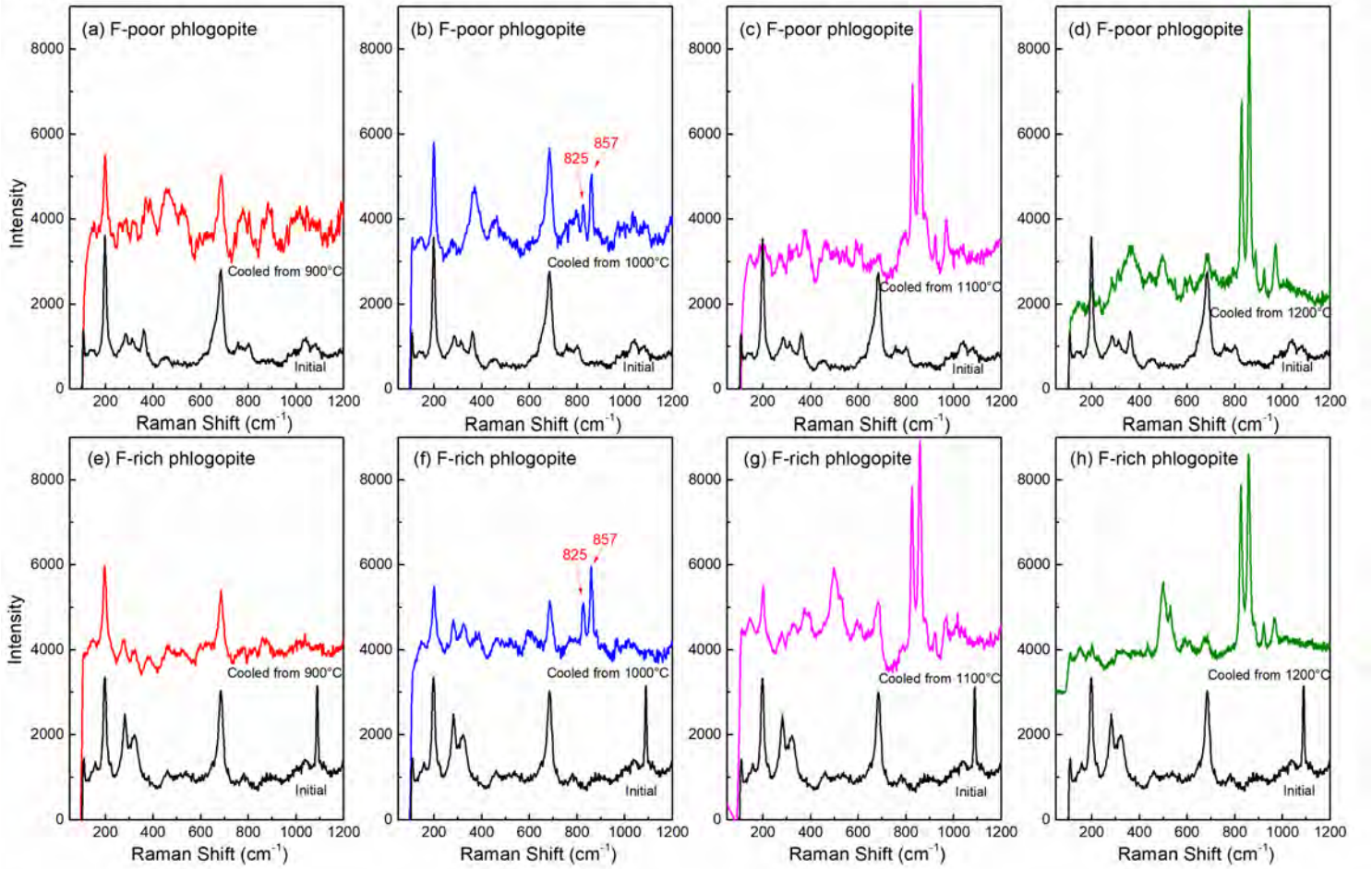

This is the peer-reviewed, final accepted version for American Mineralogist, published by the Mineralogical Society of America.
The published version is subject to change. Cite as Authors (Year) Title. American Mineralogist, in press.
DOI: https://doi.org/10.2138/am-2022-8051. http://www.minsocam.org/

Figure 3

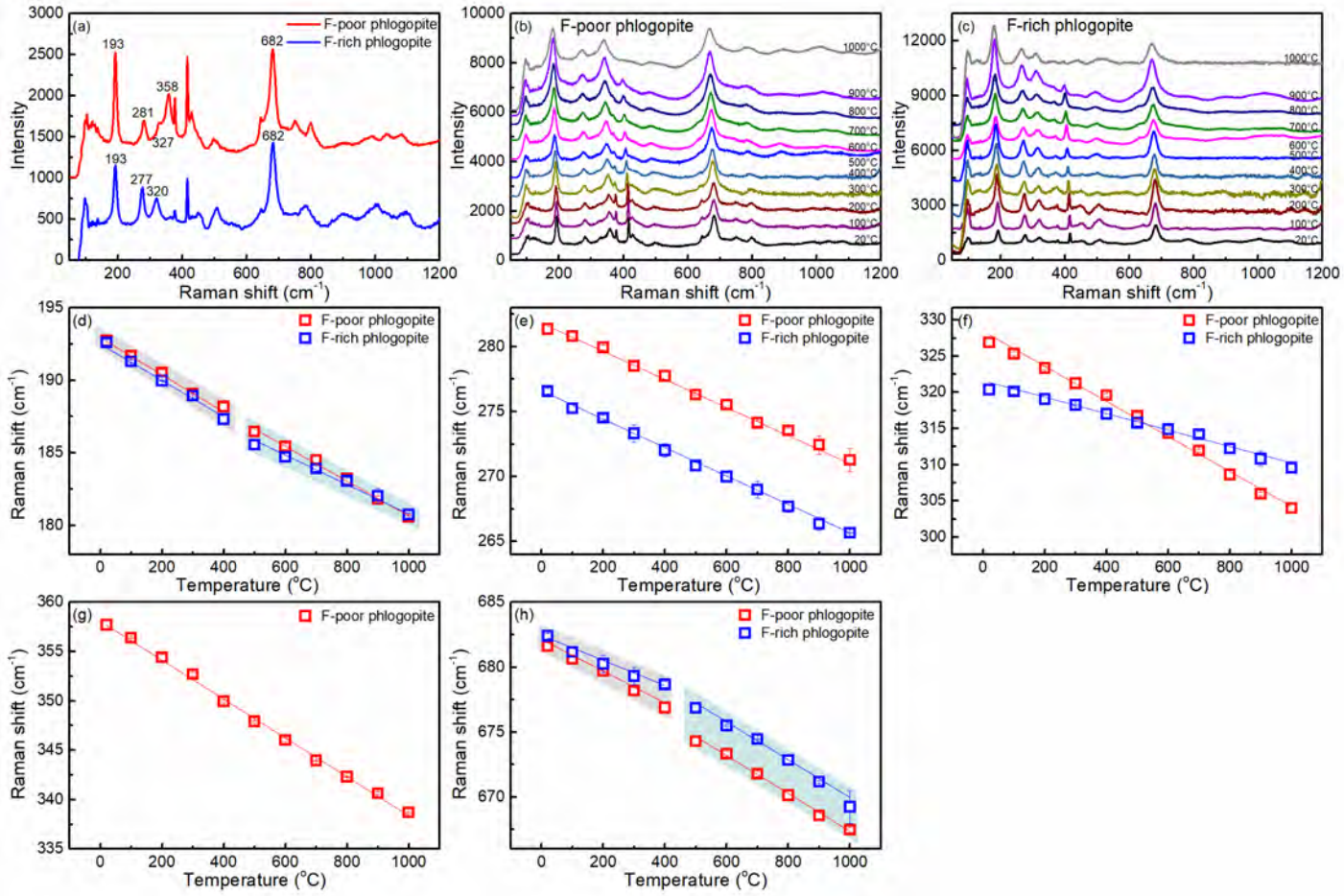

This is the peer-reviewed, final accepted version for American Mineralogist, published by the Mineralogical Society of America.
The published version is subject to change. Cite as Authors (Year) Title. American Mineralogist, in press.
DOI: https://doi.org/10.2138/am-2022-8051. http://www.minsocam.org/

Figure 4

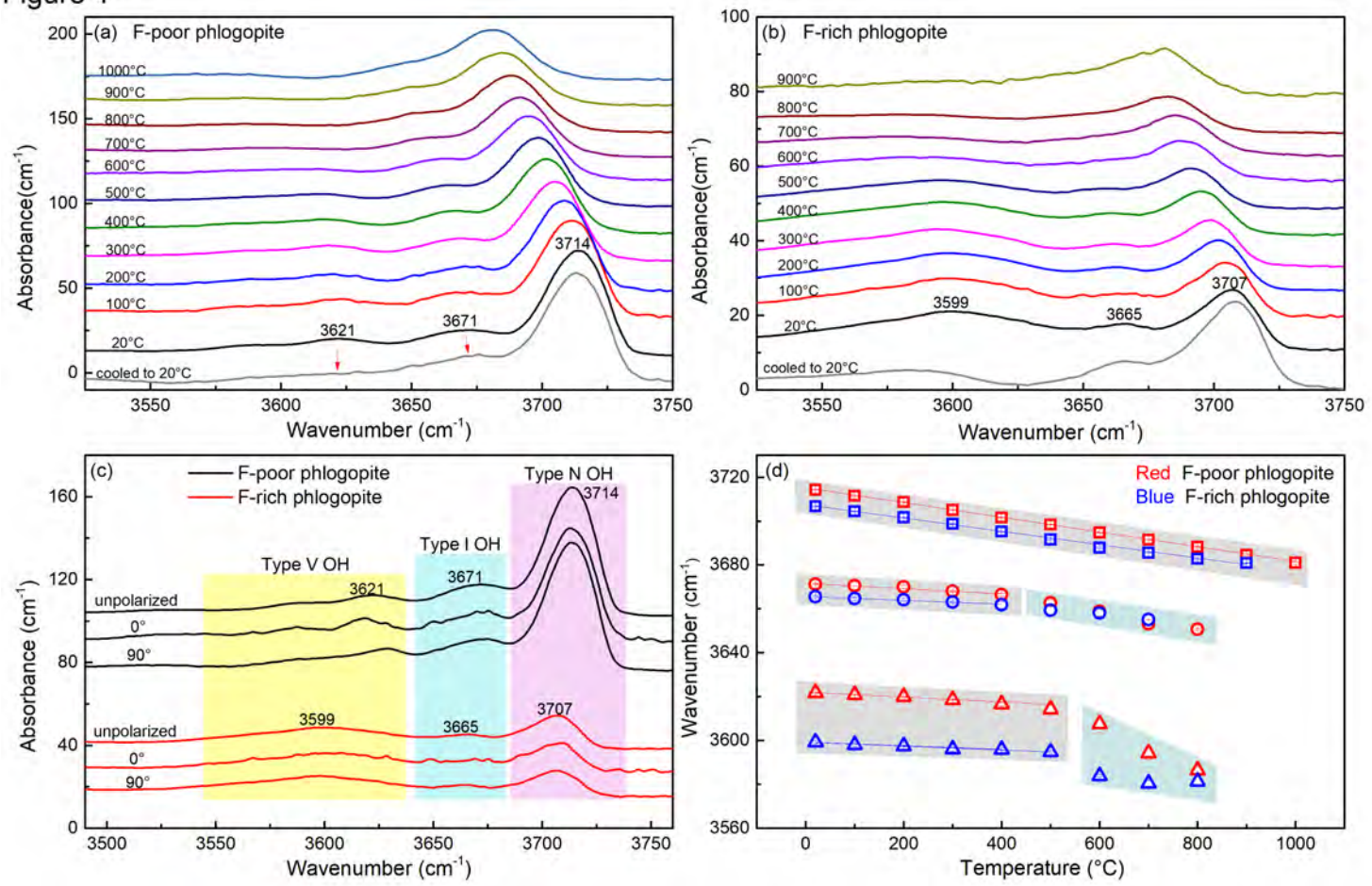

This is the peer-reviewed, final accepted version for American Mineralogist, published by the Mineralogical Society of America.
The published version is subject to change. Cite as Authors (Year) Title. American Mineralogist, in press.
DOI: https://doi.org/10.2138/am-2022-8051. http://www.minsocam.org/

Figure 5

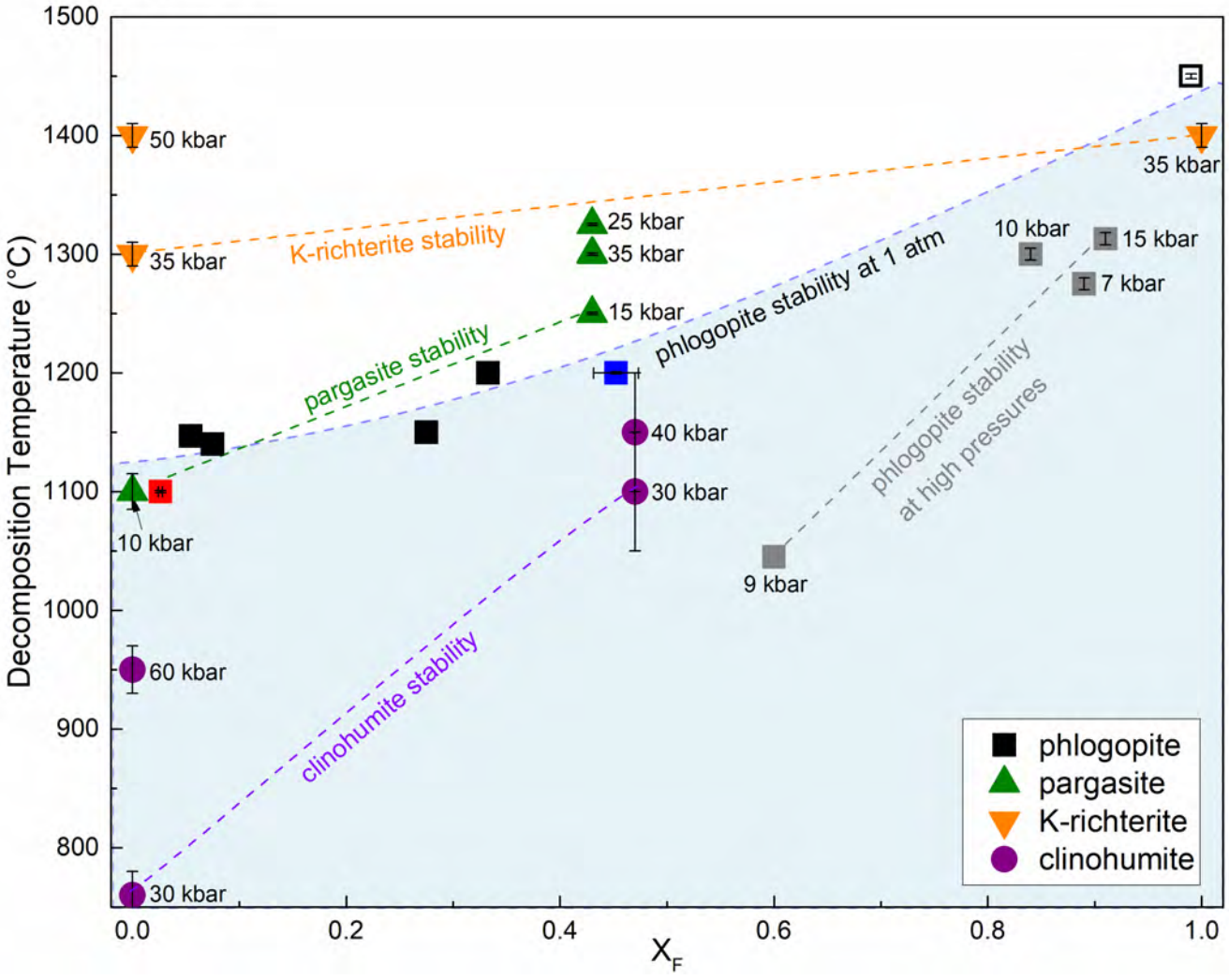

This is the peer-reviewed, final accepted version for American Mineralogist, published by the Mineralogical Society of America.
The published version is subject to change. Cite as Authors (Year) Title. American Mineralogist, in press.
DOI: https://doi.org/10.2138/am-2022-8051. http://www.minsocam.org/

Figure 6